ACS APPLIED MATERIALS & INTERFACES

Research Article

www.acsami.org

Porous Titania Nanosheet/Nanoparticle Hybrids as Photoanodes for Dye-Sensitized Solar Cells

Yang Bai,[†] Zheng Xing,[†] Hua Yu,[†] Zhen Li,[‡] Rose Amal,[§] and Lianzhou Wang*[,†]

[†]Australian Research Council (ARC) Centre of Excellence for Functional Nanomaterials, School of Chemical Engineering and Australian Institute for Bioengineering and Nanotechnology, The University of Queensland, Brisbane, Queensland 4072 Australia

[‡]Institute of Superconducting and Elctronic Materials, Australian Institute of Innovative Materials, The University of Wollongong, Northwollongong, New South Wales 2500, Australia

[§]ARC Centre of Excellence for Functional Nanomaterials, School of Chemical Engineering, The University of New South Wales, Sydney, New South Wales 2052, Australia

Supporting Information

ABSTRACT: Porous titania nanohybrids (NHs) were successfully prepared by hybridizing the exfoliated titania nanosheets with anatase TiO_2 nanoparticles. Various characterizations revealed that the titania NHs as photoanodes play a trifunctional role (light harvesting, dye adsorption, and electron transfer) in improving the efficiency (η) of the dye-sensitized solar cells. The optimized photoanode consisting layered NHs demonstrated a high overall conversion efficiency of 10.1%, remarkably enhanced by 29.5% compared to that (7.8%) obtained from the benchmark P25 nanoparticles under the same testing conditions.

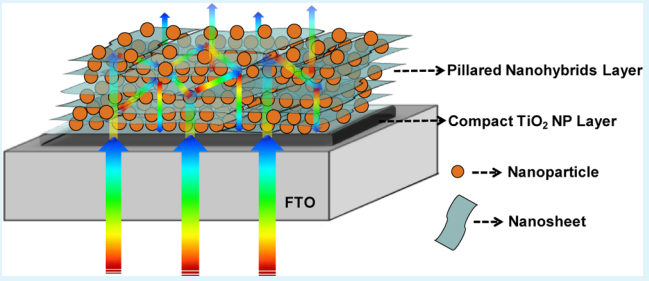

KEYWORDS: *exfoliated titania nanosheets, anatase nanoparticles, hybrid photoanodes, dye-sensitized solar cells*

INTRODUCTION

Inspired by the breakthrough work of O'Regan and Grätzel on dye-sensitized solar cells (DSSCs),[1] much effort has been made on tailoring photoanode architectures to improve the overall conversion efficiency in the past decades.[2−7] One of the major drawbacks of conventional TiO_2 nanoparticle (NP) photoanodes in DSSCs is the negligible light scattering of the films due to their small particle size ranging typically from ca. 20−30 nm, resulting in a low light-harvesting efficiency. An optical scattering layer on top has been proposed because it could enhance light harvesting by localizing the incident light within the photoanode. So far, an array of light-scattering materials has been investigated, including TiO_2 mesoporous microspheres,[7,8] hollow spheres,[9−11] and mirror-like NPs.[12,13]

Another major drawback of the conventional TiO_2 NP photoanodes is the low transport efficiency of electrons, which imposes an upper limit on the film thickness. In a film composed of TiO_2 NPs, electrons diffuse to the surface of the collector electrode (e.g., fluorine doped tin oxide (SnO_2:F) (FTO) substrate) through a zigzag pathway[14] and may easily recombine with the oxidizing species (predominately triiodide ions in the electrolyte), thus reducing the efficiency of DSSCs. Therefore, one-dimensional (1D) TiO_2[3,15−17] and ZnO nanostructures[5,14,18] and two-dimensional (2D) NSs[19,20] have attracted recent attention in facilitating electron transport in DSSCs.

Even though the light-harvesting and charge-transfer efficiencies can be enhanced by introducing an optical light-scattering layer and fabrication of films from 1D and 2D nanostructures, respectively, the surface area that is accessible to the dye is usually sacrificed, resulting in insufficient dye adsorption and thus limited conversion efficiency. Thereby how to efficiently transfer electrons and harvest light without compromising dye adsorption is believed to be one of the key challenges in achieving high-efficiency DSSCs.

Layered nanohybrids (NHs) from pillaring of semiconducting NPs such as CdS, α-Fe_2O_3, and TiO_2[21−24] into layered inorganic compounds[25−30] have recently drawn growing attention in photocatalysis as a result of their large surface area as well as suppressed electron−hole recombination because of electron transfer between the guest and host.[22,23,31] Titania NSs ($Ti_{0.91}O_2$) derived from delamination of layered compounds have unique structural characteristics of ultimate 2D anisotropy with extremely small thickness in the subnano- to nanometer scales, which leads to new physical and chemical properties for NSs.[32] In addition, the exfoliation of layered metal oxides into 2D NSs[33,34] ($Ti_{0.91}O_2$ NSs) makes it possible to pillar large-sized (TiO_2) NPs into the interlayer space of host materials through an exfoliation−restacking

Received: September 9, 2013
Accepted: October 25, 2013
Published: October 25, 2013

Scheme 1. Idealized Schematic Diagram of Photoanodes Based on Layered NHs for Light Scattering

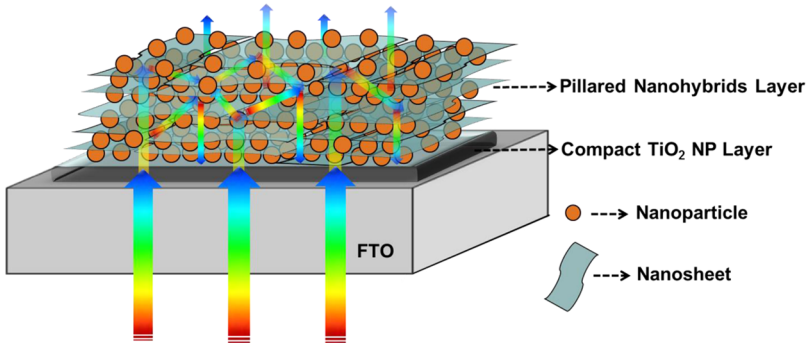

process of nanosheets and guest particles.[23,35,36] The obtained pillared NHs possess highly controllable physical and chemical properties.[22,37−39] In particular, because of the enlarged interlayer distance, the total surface area is significantly increased, facilitating chemical adsorption or reaction. Moreover, the energy band difference between the guest and host will enhance charge transfer between them.[31,40] Apart from the high surface area and enhanced electron-transfer efficiency, the large-sized 2D NSs that constitute the layered NHs can act as an ideal optical scatterer[41] as well. In this regard, the layered titania NHs are expected to be promising photoanode candidates, playing a trifunctional role (light harvesting, dye adsorption, and electron transfer) for high-efficiency DSSCs.

In this work, we report the layered NHs prepared by hybridizing the exfoliated titania NSs ($Ti_{0.91}O_2$) with the anatase TiO_2 NPs, as shown in S-Figure 1 in the Supporting Information (SI) for use as photoanodes in DSSCs. Our key strategy is to use an exfoliation−reassembly strategy to introduce TiO_2 NPs ranging from 7 to 9 nm (S-Figure 2b in the SI) into the interlayers of 2D exfoliated $Ti_{0.91}O_2$ NSs (S-Figure 2a in the SI) without deterioration of their fundamental crystal structures. In this way, the porosity and surface area of the NHs are expected to be significantly enlarged, which is beneficial for sufficient dye adsorption, and submicrometer-sized NSs like the light shield will play a vital role in increasing the light scattering, as shown in the idealized Scheme 1. In addition, we hypothesize that the electron−hole recombination would be effectively suppressed because of charge transfer between the guest and host in the layered NH system.[22,23,31] An enhanced overall conversion efficiency of 10.1% for a layered titania NS/NP hybrid photoanode was achieved, a noticeable 29.5% improvement compared with the photoelectrode made of the benchmark Degussa TiO_2 P25 under the same testing conditions. Various characterizations confirmed our hypothesis and the feasibility of using new layered NH photoanodes for efficiency improvement of DSSCs.

EXPERIMENTAL SECTION

Preparation of Titania NS/NP NHs. A titania NS ($Ti_{0.91}O_2$) suspension was prepared according to Sasaki's method.[35,36,42,43] Layered titanate precursor $Cs_{0.68}Ti_{1.83}O_4$ was first prepared via a solid-state reaction. In a typical synthesis, Cs_2CO_3 (7.694 g) and TiO_2 (10.0 g) powders were ground for at least 0.5 h to obtain an adequate mixture. The mixture was transferred to an alumina crucible and calcined at 760 °C for 30 min. The mixed powder was then reground for 0.5 h and recalcined at 760 °C for 12 h. The obtained $Cs_{0.68}Ti_{1.83}O_4$ powder was subsequently proton-exchanged with an excess amount of HCl (1 M) for 3 days, and the HCl solution was refreshed every 24 h. The protonated titanate precursor $H_{0.68}Ti_{1.83}O_4 \cdot H_2O$ was dispersed in a tetrabutylammonium hydroxide solution containing the same amount of protons intercalated in the layered titanate. The white suspension was then shaken for over 1 week. To remove the unexfoliated titanates, the suspension was centrifuged under 4700 rpm for 5 min and the supernatant suspension was collected for use. The obtained $Ti_{0.91}O_2$ titania NS suspension has a concentration of around 1.79 g/L.

Anatase NPs were prepared via a hydrolysis method. In a typical preparation process, 1-propanol (19.9 mL) and titanium isopropoxide (43.8 mL) were first mixed. The mixed solution was then dropwise added to 300 mL of a diluted HNO_3 solution (0.055 M) under vigorous stirring, and a white suspension can be observed. The white suspension was kept at 70−80 °C in a water bath for 8 h until an opaque white suspension was obtained. Thereafter, the opaque white suspension was ultrasonicated by an ultrasonication probe for 30 min. The anatase NP suspension had a concentration of 0.407 M. To prepare the anatase NP paste, a diluted ammonia solution was added dropwise to the suspension under stirring until precipitates appeared. The top clear water was removed after standing for several hours, and then the precipitates were dried at 50 °C.

Titania NHs between NSs and anatase NPs were synthesized as follows: under vigorous stirring, an anatase NP suspension (8.8 mL) was added to a NS suspension (40 mL) dropwise. The suspension was then kept under 60 °C overnight. To obtain the NHs, the suspension was centrifuged and washed with distilled water and ethanol several times.

Preparation of TiO_2 Photoanodes. To prepare the DSSC photoanodes, an FTO substrate (2.2 mm thickness, 8 Ω/sq, Dyesol Glass) was cleaned with 2-propanol in an ultrasonic bath for 30 min, followed by thorough rinsing with water. A compact layer (ca. 110 nm) was first prepared by dip-coating a TiO_2 organic sol[44] on the cleaned FTO surface, which not only has a blocking effect but also can improve adherence between the TiO_2 layer and FTO substrates. As described in our previous work,[45] TiO_2 pastes of various samples including P25, anatase NP, and layered titania NHs were prepared, then deposited on the FTO glass pretreated with a TiO_2 organic sol[44] by the doctor-blade method,[45] and kept in a clean box for at least 15 min before heat treatment to reduce the surface irregularity and mechanical stress of the pastes. The working electrodes were put into a muffle furnace and heated at 450 °C for 30 min. Finally, all of the films were post-treated again with TiO_2 organic sol.

Characterization of the Layered NH Powder and Films. The crystalline phases and structures of the samples were determined by using a Bruker Advanced X-ray diffractometer (40 kV and 30 mA) with Cu Kα_1 (λ = 0.15406 nm) radiation. The morphologies of the layered NH powder and films were examined by transmission electron microscopy (TEM; Tecnai Field Emission F20) and scanning electron microscopy (SEM; JEOL 6300). Brunauer−Emmett−Teller (BET) surface areas (S_{BET}) were analyzed with a nitrogen adsorption apparatus (Quadrasorb SI). The film powder was obtained by scratching calcined films off of the FTO glass, and all samples were degassed at 200 °C overnight before measurement. Dye desorption was performed by immersing the dye-sensitized films in 0.1 M NaOH in an ethanol−water (1:1, v/v) solution.[9] The dye-uptake capacity of

each photoanode was determined from the absorption value for each NaOH/dye solution by an UV−vis spectrophotometer (Shimadzu UV-2450). The scattering and absorption properties of all samples were investigated with an UV−vis diffuse-reflectance/light-absorption spectrometer (Shimadzu UV-2450).

Fabrication and Measurements of DSSCs. Dye loading was performed by immersing the working electrodes into a 0.5 mM N719 (Dyesol) dye solution in a 1:1 (v/v) mixture of acetonitrile and *tert*-butanol and kept for 12−14 h. Counter electrodes were fabricated by spin-coating a H_2PtCl_6−isopropanol solution (5 mM) onto FTO substrates and heating at 380 °C for 15 min.[44] Then the dye-sensitized working electrode and platinum counter electrode were assembled into a sandwich-type cell, as described in our previous work.[46]

The photocurrent density−voltage (J−V) curves were recorded by using an Oriel AM 1.5 solar simulator equipped with an AM 1.5G type filter (Newport, 81094) and a Keithley model 2420 digital source meter. The dark-current scan was performed in similar conditions but without illumination. The incident photon-to-current conversion efficiency (IPCE) plotted as a function of the excitation wavelength was obtained by using a Newport 1918-c power meter under irradiation of a 300 W Oriel xenon light source with an Oriel Cornerstone 260 $^1/_4$ m monochromator in direct-current mode.[14] Open-circuit voltage decay (OCVD) was carried out by switching off illumination on the DSSC in a steady state and monitoring the decay of the open-circuit voltage (V_{oc}).[20] Electrochemical impedance spectroscopy (EIS) was mearsured by a Solartron 1480 potentiostat in a frequency range of 10^6−0.1 Hz in the dark, and the applied bias voltage and alternating-current amplitude were set as −0.7 V and 10 mV, respectively.[14]

RESULTS AND DISCUSSION

Characterization of the Layered NH Powder and Various Films. The resultant layered NH powder and various films were comprehensively characterized, and Figure 1 shows

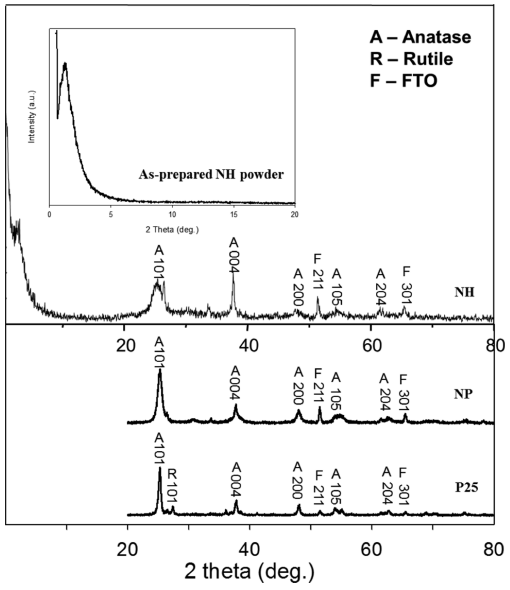

Figure 1. XRD patterns of P25, TiO_2 NPs, and layered titania NH films on FTO substrates and an as-prepared layered titania NH powder.

X-ray diffraction (XRD) patterns of the as-prepared NH powder and films prepared with P25, sol−gel-derived TiO_2 NPs, and NH samples printed on FTO substrates. As indicated in the XRD patterns, both the NP and NH samples are of the pure anatase (A) phase (JCPDS no. 21-1272) with typical peaks (101), (004), and (200), whereas all diffraction peaks of the P25 films can be well indexed to a mixture of anatase (A) TiO_2 and rutile (R) TiO_2 (JCPDS no. 21-1276). Peaks F belong to FTO substrates. The Raman spectrum of the NH film further confirmed the anatase phase with typical vibrational bands, as marked on S-Figure 4 in the SI. The inset shows a poorly-resolved 001 index (2θ = 1.24°) for the as-prepared NH, which can be attributed to the formation of a disordered porous titania heterostructure consisting of NSs and NPs in some domains. An electrostatic interaction between negatively charged titania NSs and positively charged TiO_2 NPs is believed to be a driving force for the formation of such a type of disordered heterostructure.[22] The discernible broad 010 reflection for the NH film after heat treatment shifted toward the higher angle side (2θ = 2.46°), indicative of shrinkage in the the basal spacing mainly attributed to dehydroxylation of TiO_2 nanosol particles but maintenance of the NH structure.

The formation of the layered NH structure was further confirmed using TEM analysis. Figure 2a and S-Figure 3 in the

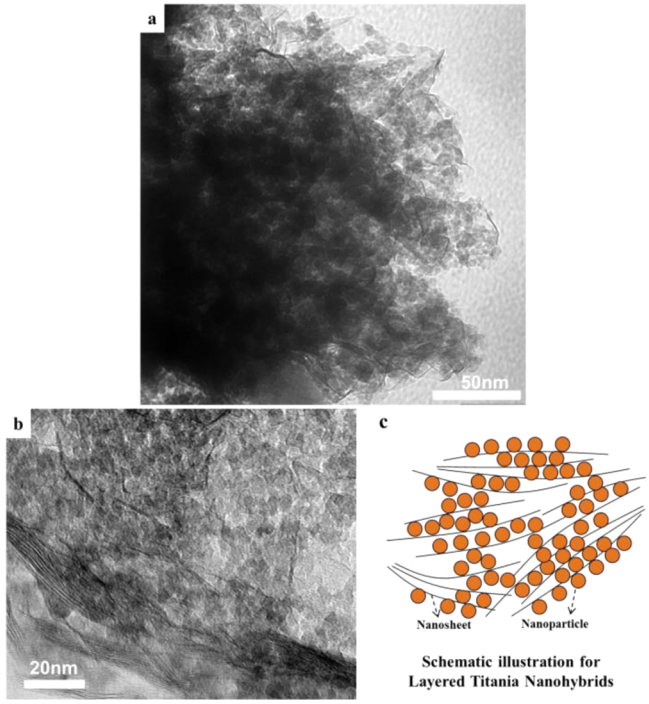

Figure 2. (a) Typical TEM image of the restacked NH sample. (b) High-magnification TEM image showing the lamellar structure. (c) Schematic illustration of layered titania NHs.

SI depict the typical TEM images of restacked NHs. The high-resolution TEM image in Figure 2b exhibits an assembly of parallel dark lines ($Ti_{0.91}O_2$ NSs) and spherical shapes (TiO_2 NPs) in some domains. Unlike the highly ordered pillared structure prepared from the restacking of exfoliated NSs with small-sized guest species such as Li^+ and Al_{13}^+ clusters,[47,48] it is understandable that the restacking of larger TiO_2 NPs with extremely thin NSs is much more difficult to control, thus leading to a poorly ordered layered structure. As shown in Figure 2a,b, the exfoliated $Ti_{0.91}O_2$ NSs are randomly hybridized with TiO_2 NPs, which is in good agreement with the XRD results. Figure 2c is an idealized schematic illustration of the highly disordered NH structure for better understanding.

In order to further verify the disordered layered structure in the calcined films, SEM characterization was carried out to

observe the resultant structures. The platelike surface of the NH film (Figure 3a) is quite different from that of P25 and NP

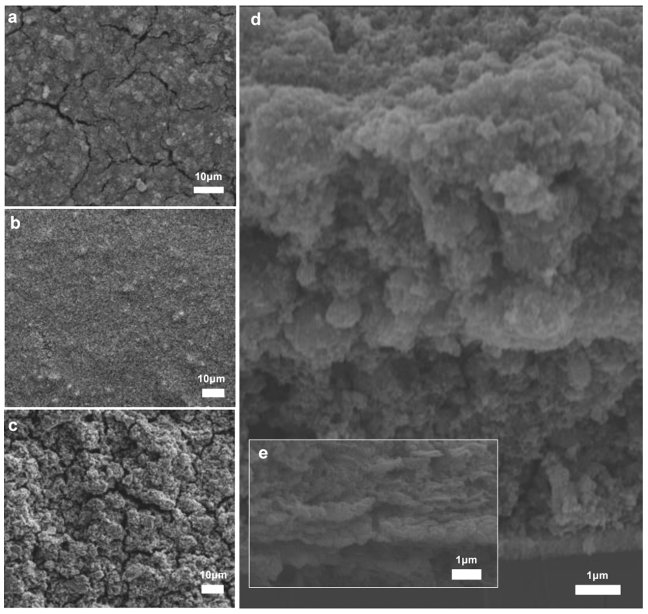

Figure 3. Surface SEM images of (a) layered NH, (b) P25, and (c) NP films. (d) Cross-sectional SEM images of a whole layered NH film. (e) High-magnification cross-sectional SEM images of a randomly selected area in the layered NH film showing the layered structure.

films (Figure 3b,c). Although some microcracks can be found in SEM images, to some extent, this can be optimized by a following post-treatment step with TiO_2 sol. The optical property (which will be discussed later) also confirms that the light harvesting of the films was not affected much by such microcracks. As shown in the cross-sectional image (Figure 3d), all of the films have a thickness of ca.12.3 μm. High-magnification cross-sectional images were taken randomly through the whole cross section of the NH films. Upon heat treatment, a disordered micrometer-thick layer will be formed, consisting of several layers of NSs and NPs. As shown in Figure 3e, the micrometer-thick layered structure can be clearly visualized within the NH film after calcination.

The nitrogen adsorption–desorption isotherms of an as-prepared NH powder and a film powder scratched off from the calcined NH films shown in Figure 4 provide further evidence for the formation of a porous layered structure by reassembling exfoliated $Ti_{0.91}O_2$ NSs in the presence of anatase NPs. The NH shows a type IV isotherm, characteristic of the mesoporous structure in the materials. This clearly reveals that the mesopores in the NHs were developed by random hybridization of $Ti_{0.91}O_2$ NSs with anatase NPs. In addition, the mesoporous NHs show the type H3 hysteresis loop in the IUPAC classification, suggesting that slit-shaped pores were formed. As shown in Figure 4, the BET specific surface area of the as-prepared samples was quite high (287 m^2/g), and the film powder decreased to 167 m^2/g as a result of heat treatment at 450 °C.

Diffuse Reflectivity and UV–Vis Absorption. The reflectivity of each film was studied to investigate the scattering effect of the layered NHs. Figure 5 shows the diffuse-reflectance spectra of various samples. Apparently, layered NH films had much higher reflectivity in the wavelength range of 380–800 nm than that of NP and P25 films. This evidence confirms our

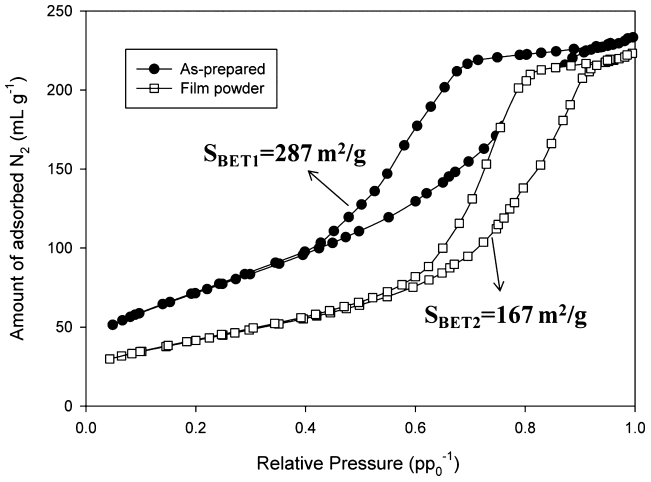

Figure 4. Nitrogen adsorption–desorption isotherms of an as-prepared layered NH powder and a powder scratched off from the calcined NH films.

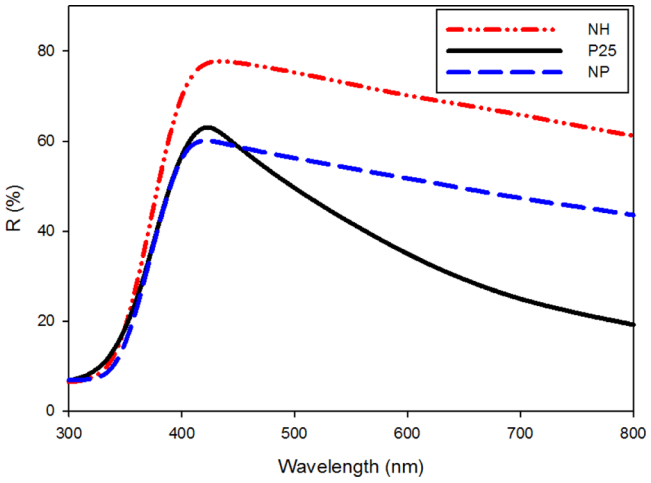

Figure 5. Diffuse-reflectance spectra of the P25, NPs, and layered NH films.

hypothesis on the efficient light scattering of layered NHs acting as light shields. Note that the reflectivity of the NP film is slightly higher than that of the P25 film in the same wavelength range, possibly because of the aggregation of sol–gel-prepared NPs (Figure 3c). In order to study the photovoltaic properties of DSSCs based on the layered NHs, dye loading was first investigated (Table 1). Prior to dye-loading measurement,

Table 1. Comparison of the Photovoltaic Properties, BET Surface Areas, and Dye Loading of P25, NPs, and Layered NH Photoanodes

sample	J_{sc} [mA/cm^2]	V_{oc} [V]	FF [%]	η^a [%]	S_{BET} value [m^2/g]	dye loading^b [10^{-7} mol/cm^2]
P25	16.4	0.73	65	7.8	51	1.80
NP	15.9	0.73	64	7.4	43	1.65
NH	19.2	0.75	70	10.1	167	2.05

[a]Measurements were performed under AM 1.5G one sun (light intensity: 100 mW/cm^2), the active areas were ca. 0.16 cm^2 for all of the cells, and the average value of each data was obtained by testing 6–8 cells. [b]Dye-absorbed films with a dimension of ca. 3 cm^2 were used for estimating the dye uptake.

UV−vis absorption was carried out for all three different films with dye adsorbed as shown in Figure 6. Compared with the

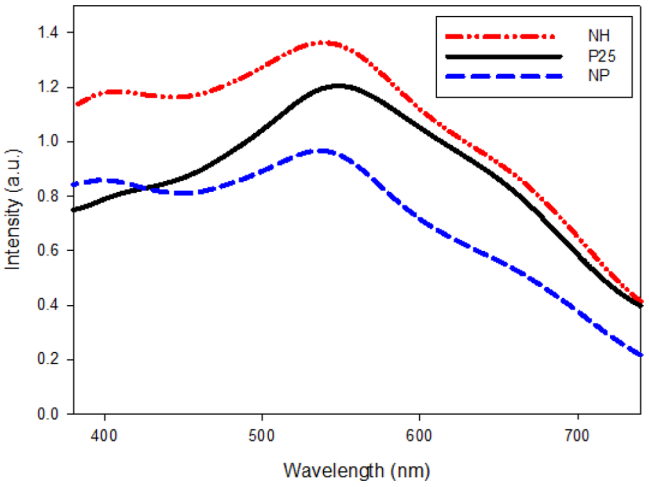

Figure 6. UV−vis absorption spectra of the P25, NPs, and layered NH films with dye adsorbed.

TiO_2 NP films (NP and P25), the layered NH films showed a higher absorption in the wavelength range from 400 to 700 nm, which is consistent with the significantly increased dye loading indicated in Table 1 and corresponding photographs as shown in S-Figure 5 in the SI. In addition, we found that upon monolayer adsorption[49,50] the dye-loading amount is quite comparable with those reported in other literatures.[7,9,17] This higher dye loading can be attributed to the large surface area of the layered NH films, as verified by BET specific surface area (S_{BET}) measurements (Table 1).

***J−V* Characteristics.** The photovoltaic performance of a layered NH photoelectrode was analyzed against the photoelectrodes fabricated with P25 and NP, as listed in Table 1, with the short *J−V* characteristics of DSSCs shown in Figure 7a. Table 1 compares the photovoltaic properties of DSSCs based on various films with a thickness of ca. 12.3 μm. Because of insufficient light harvesting and inefficient electron transfer, DSSCs assembled with P25 showed a limited efficiency of 7.8% (comparable with the efficiency reported in the literature[9,12,51] as well as that of devices made from Dyesol paste shown in S-Figure 7 in the SI), with relatively small J_{sc} (16.4 mA/cm^2), V_{oc} (0.73 V), and fill factor (FF; 65%). Whereas all of the key parameters of DSSCs based on layered NHs were improved (J_{sc} = 19.2 mA/cm^2, V_{oc} = 0.75 V, and FF = 70%), which resulted in an enhanced overall conversion efficiency (η) of 10.1% (close to the champion efficiency of 12.3%[52]). The possible explanation for the higher V_{oc} of the hybrid cells is the blocking of recombination as a result of charge transfer[22,23,30,31,53,54] within the layered NH film, which results in an increase in the electron density in TiO_2 and thus a shift of the Fermi level.[55] As evidenced above, the large surface area makes it accessible for more dye adsorption, and the light-scattering effect of the reassembled exfoliated titanates favors an enhanced light-harvesting efficiency by increasing the optical length serving as a light-scattering shield, and thereby enhanced J_{sc} for the cell with the layered NH film.[5,56] The faster electron diffusion rate[57,58] in the NH film can be considered as a reason for the higher FF of the cell assembled with NH films, compared with the cell using the P25 film.

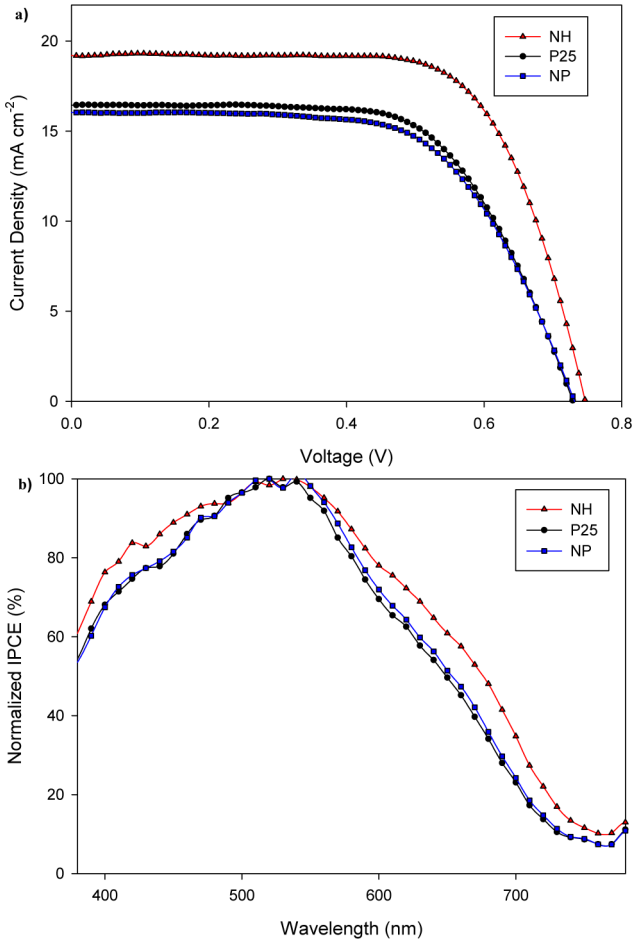

Figure 7. (a) *J−V* curves and (b) normalized IPCE of DSSCs based on P25, NPs, and layered NH photoanodes.

Note that the DSSC made of an anatase NP film showed slightly decreased J_{sc} and η. This could be mainly caused by the lower dye loading in this NP film because of the decreased surface area as a result of aggregation, whereas in the case of the layered NH sample, the randomly hybridized layered $Ti_{0.91}O_2$ inhibits TiO_2 NP growth upon calcination.

IPCE Performance. The IPCE spectra of the various photoanodes as a function of the illumination wavelength can provide further evidence on the scattering effect of the NH structure. The IPCE of the NH-film-based DSSCs (S-Figure 6 in the SI) showed a considerable increase over the entire wavelength range. To better determine the superior optical characteristic of the titania NHs, the normalized IPCE was obtained by normalizing the measured IPCE to the maximum intensity of 520 nm, as shown in Figure 7b. We can then clearly visualize the impact of this new NH structure on the light conversion efficiency of the lower-energy photons in the long-wavelength range, from 560 nm until far in the absorption tail (up to 750 nm). The full spectrum enhancement of NH devices compared with that of P25 and NP should be evidently attributed to the increased dye adsorption (large surface area) and efficient light scattering (NS components).

Dark Current, OCVD, and EIS. To further investigate the origin and evidence for the enhanced efficiency, especially the improved V_{oc} and FF of the layered NH-based cells, the dark-current potential scans were performed, as shown in Figure 8a, which was employed to estimate the charge-carrier recombina-

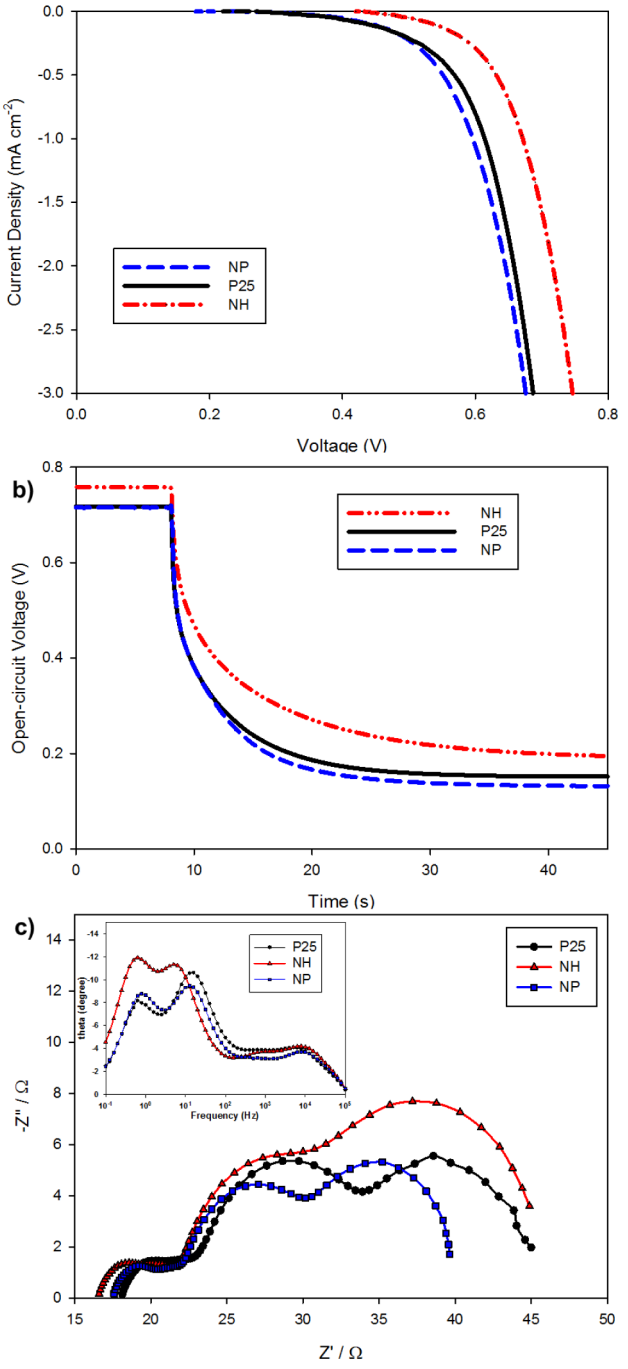

Figure 8. (a) Dark-current potential scans, (b) OCVD profiles, and (c) impedance spectra of DSSCs based on P25, NPs, and layered NH photoanodes. The Bode phase plot is shown in the inset of part c.

tion in DSSCs. It is generally believed that electron recombination is attributed to the reduction of I_3^- ions by electrons on the FTO substrate, which will result in a decrease in the photocurrent.[59] Compared with the NP and P25 films, the onset of the dark current for DSSCs with the layered NH film occurred at a higher potential, and a smaller dark current was produced under the same bias above 0.4 V. This result indicates a slower recombination rate between the transferred electrons and I_3^- ions for the NH film.[60,61] Since suppression of the back electron transfer in the layered NHs, increased V_{oc} and FF were achieved and consequently improved the overall conversion efficiency.

The OCVD technique was employed to further examine the charge-transfer kinetics of the DSSCs. Before the measurement, a steady-state voltage for the DSSC cell was obtained under illumination, and the subsequent decay of V_{oc} was then recorded after illumination was interrupted. The decay of V_{oc} can be viewed as a sign of electron loss as a result of the electron−hole recombination.[20,62] As shown in Figure 8b, the decay rate of V_{oc} is apparently slower in DSSCs assembled with the layered NHs, implying a reduced charge recombination rate in comparison with that of DSSCs fabricated by anatase NP and P25, which is in good agreement with the result in Figure 8a.

To better elucidate the electron transport and charge recombination in NH photoelectrodes, EIS was performed in the dark under a forward bias of −0.7 V, as shown in Figure 8c, and the inset shows the Bode phase plot. As observed in the Nyquist plots, the radius of the middle semicircle increases in the order NP < P25 < NH, implying a larger electron recombination resistance for NH electrodes.[63] In addition, the middle-frequency peak of DSSCs based on NH electrodes shown in the Bode phase plots shifts to lower frequency relative to P25 and NP, which indicates that the electron lifetime was prolonged in NH-based DSSCs.[64] Therefore, the larger electron recombination resistance and longer electron lifetime observed in NH relative to P25- and NP-based DSSCs illustrate more effective suppression of the back-reaction of the injected electron with I_3^- in the electrolyte due to electron transfer between the guest and host[22,23,31] and better explained the observed improvements in both the photocurrent and photovoltage, yielding a substantially enhanced energy conversion efficiency.[63]

CONCLUSIONS

In summary, a new type of porous layered titania NH was successfully prepared by hybridizing the exfoliated titanate with the anatase TiO_2 nanosol, which was subsequently used as a trifunctional photoanode for high-efficiency DSSCs. Reflectance spectra demonstrate that the light-harvesting efficiency of the NH films was significantly higher than that of the P25 film because of the effective light scattering of $Ti_{0.91}O_2$ NS. The larger surface area of the layered NH films, leading to increased dye loading, is verified by BET specific surface area measurements. In addition, not only the dark-current potential scan but also the OCVD indicates a lower charge recombination for a photoelectrode fabricated with NHs. The DSSCs assembled using photoanodes with layered NHs demonstrated a high overall conversion efficiency of 10.1%, remarkably enhanced by 29.5% compared to that (7.8%) obtained from the benchmark P25 NPs. Layered NHs may lead to a new way to fine-tune the photoanode structures for high-efficiency DSSCs as well as boost the efficiency of quantum-dot-sensitized solar cells.

ASSOCIATED CONTENT

Supporting Information

Schematic diagram for an exfoliation−hybridization route to prepare layered titania NHs, TEM images, Raman spectra, corresponding photographs of NP, P25, and NH films after dye adsorption, IPCE of DSSCs, and *J*−*V* curves. This material is available free of charge via the Internet at http://pubs.acs.org.

AUTHOR INFORMATION

Corresponding Author

*E-mail: l.wang@uq.edu.au.

Notes

The authors declare no competing financial interest.

■ ACKNOWLEDGMENTS

This work was financially supported by the ARC through Discovery Projects. Y.B. acknowledges support from the Chinese Scholarship Council.

■ REFERENCES

(1) O'Regan, B.; Grätzel, M. *Nature* **1991**, *353* (6346), 737−740.
(2) Ko, S. H.; Lee, D.; Kang, H. W.; Nam, K. H.; Yeo, J. Y.; Hong, S. J.; Grigoropoulos, C. P.; Sung, H. J. *Nano Lett.* **2011**, *11* (2), 666−671.
(3) Liu, B.; Aydil, E. S. *J. Am. Chem. Soc.* **2009**, *131* (11), 3985−3990.
(4) Zhang, Q. F.; Chou, T. P.; Russo, B.; Jenekhe, S. A.; Cao, G. Z. *Angew. Chem., Int. Ed.* **2008**, *47*, 2402−6.
(5) Law, M.; Greene, L. E.; Johnson, J. C.; Saykally, R.; Yang, P. *Nat. Mater.* **2005**, *4* (6), 455−459.
(6) Zhu, K.; Neale, N. R.; Miedaner, A.; Frank, A. J. *Nano Lett.* **2007**, *7* (1), 69−74.
(7) Huang, F. Z.; Chen, D. H.; Zhang, X. L.; Caruso, R. A.; Cheng, Y. B. *Adv. Funct. Mater.* **2010**, *20* (8), 1301−1305.
(8) Yan, K. Y.; Qiu, Y. C.; Chen, W.; Zhang, M.; Yang, S. H. *Energy Environ. Sci.* **2011**, *4* (6), 2168−2176.
(9) Wu, X.; Lu, G. Q.; Wang, L. *Energy Environ. Sci.* **2011**, *4* (9), 3565−3572.
(10) Koo, H. J.; Kim, Y. J.; Lee, Y. H.; Lee, W. I.; Kim, K.; Park, N. G. *Adv. Mater.* **2008**, *20* (1), 195−199.
(11) Qian, J. F.; Liu, P.; Xiao, Y.; Jiang, Y.; Cao, Y. L.; Ai, X. P.; Yang, H. X. *Adv. Mater.* **2009**, *21* (36), 3663−3667.
(12) Yu, H.; Bai, Y.; Zong, X.; Tang, F. Q.; Lu, G. Q. M.; Wang, L. Z. *Chem. Commun.* **2012**, *48* (59), 7386−7388.
(13) Zhang, H. M.; Han, Y. H.; Liu, X. L.; Liu, P.; Yu, H.; Zhang, S. Q.; Yao, X. D.; Zhao, H. J. *Chem. Commun.* **2010**, *46* (44), 8395−8397.
(14) Bai, Y.; Yu, H.; Li, Z.; Amal, R.; Lu, G. Q.; Wang, L. Z. *Adv. Mater.* **2012**, *24* (43), 5850−5856.
(15) Ohsaki, Y.; Masaki, N.; Kitamura, T.; Wada, Y.; Okamoto, T.; Sekino, T.; Niihara, K.; Yanagida, S. *Phys. Chem. Chem. Phys.* **2005**, *7* (24), 4157−4163.
(16) Zhu, K.; Vinzant, T. B.; Neale, N. R.; Frank, A. J. *Nano Lett.* **2007**, *7* (12), 3739−3746.
(17) Adachi, M.; Murata, Y.; Takao, J.; Jiu, J. T.; Sakamoto, M.; Wang, F. M. *J. Am. Chem. Soc.* **2004**, *126* (45), 14943−14949.
(18) Xu, F.; Sun, L. *Energy Environ. Sci.* **2011**, *4* (3), 818−841.
(19) Lin, C. Y.; Lai, Y. H.; Chen, H. W.; Chen, J. G.; Kung, C. W.; Vittal, R.; Ho, K. C. *Energy Environ. Sci.* **2011**, *4* (9), 3448−3455.
(20) Wu, X.; Chen, Z. G.; Lu, G. Q.; Wang, L. Z. *Adv. Funct. Mater.* **2011**, *21* (21), 4167−4172.
(21) Fujishiro, Y.; Uchida, S.; Sato, T. *Int. J. Inorg. Mater.* **1999**, *1* (1), 67−72.
(22) Kim, T. W.; Hur, S. G.; Hwang, S. J.; Park, H.; Choi, W.; Choy, J. H. *Adv. Funct. Mater.* **2007**, *17* (2), 307−314.
(23) Choy, J. H.; Lee, H. C.; Jung, H.; Kim, H.; Boo, H. *Chem. Mater.* **2002**, *14* (6), 2486−2491.
(24) Geng, F.; Ma, R.; Nakamura, A.; Akatsuka, K.; Ebina, Y.; Yamauchi, Y.; Miyamoto, N.; Tateyama, Y.; Sasaki, T. *Nat. Commun.* **2013**, *4*, 1632.
(25) Paek, S.-M.; Jung, H.; Park, M.; Lee, J.-K.; Choy, J.-H. *Chem. Mater.* **2005**, *17* (13), 3492−3498.
(26) Shibata, T.; Takanashi, G.; Nakamura, T.; Fukuda, K.; Ebina, Y.; Sasaki, T. *Energy Environ. Sci.* **2011**, *4* (2), 535−542.
(27) Ko, J.; Kim, I.; Hwang, S.; Jung, H. *J. Nanosci. Nanotechnol.* **2011**, *11* (2), 1726.
(28) Xu, B.-H.; Lin, B.-Z.; Wang, Q.-Q.; Pian, X.-T.; Zhang, O.; Fu, L.-M. *Microporous Mesoporous Mater.* **2012**, *147* (1), 79−85.
(29) Lin, B.; He, L.; Zhu, B.; Chen, Y.; Gao, B. *Catal. Commun.* **2012**, *29* (0), 166−169.
(30) Lin, B.-Z.; Li, X.-L.; Xu, B.-H.; Chen, Y.-L.; Gao, B.-F.; Fan, X.-R. *Microporous Mesoporous Mater.* **2012**, *155* (0), 16−23.
(31) Yanagisawa, M.; Uchida, S.; Fujishiro, Y.; Sato, T. *J. Mater. Chem.* **1998**, *8* (12), 2835−2838.
(32) Liu, G.; Wang, L.; Yang, H. G.; Cheng, H.-M.; Lu, G. Q. *J. Mater. Chem.* **2010**, *20* (5), 831−843.
(33) Akatsuka, K.; Takanashi, G.; Ebina, Y.; Haga, M.-a.; Sasaki, T. *J. Phys. Chem. C* **2012**, *116* (23), 12426−12433.
(34) Osada, M.; Sasaki, T. *ECS Trans.* **2013**, *50* (6), 111−116.
(35) Sasaki, T.; Watanabe, M.; Hashizume, H.; Yamada, H.; Nakazawa, H. *J. Am. Chem. Soc.* **1996**, *118* (35), 8329−8335.
(36) Sasaki, T.; Watanabe, M. *J. Am. Chem. Soc.* **1998**, *120* (19), 4682−4689.
(37) Paek, S. M.; Jung, H.; Lee, Y. J.; Park, M.; Hwang, S. J.; Choy, J. H. *Chem. Mater.* **2006**, *18* (5), 1134−1140.
(38) Kim, T. W.; Ha, H. W.; Paek, M. J.; Hyun, S. H.; Baek, I. H.; Choy, J. H.; Hwang, S. J. *J. Phys. Chem. C* **2008**, *112* (38), 14853−14862.
(39) Kim, T. W.; Hwang, S. J.; Jhung, S. H.; Chang, J. S.; Park, H.; Choi, W.; Choy, J. H. *Adv. Mater.* **2008**, *20* (3), 539−542.
(40) Choy, J. H.; Lee, H. C.; Jung, H.; Kim, H.; Boo, H. *Chem. Mater.* **2002**, *14* (6), 2486−2491.
(41) Qiu, Y. C.; Chen, W.; Yang, S. H. *J. Mater. Chem.* **2010**, *20* (5), 1001−1006.
(42) Sasaki, T.; Ebina, Y.; Kitami, Y.; Watanabe, M.; Oikawa, T. *J. Phys. Chem. B* **2001**, *105* (26), 6116−6121.
(43) Liu, G.; Wang, L. Z.; Sun, C. H.; Chen, Z. G.; Yan, X. X.; Cheng, L. N.; Cheng, H. M.; Lu, G. Q. *Chem. Commun.* **2009**, *0* (11), 1383−1385.
(44) Yu, H.; Zhang, S. Q.; Zhao, H. J.; Will, G.; Liu, P. *Electrochim. Acta* **2009**, *54* (4), 1319−1324.
(45) Mills, A.; Elliott, N.; Hill, G.; Fallis, D.; Durrant, J. R.; Willis, R. L. *Photochem. Photobiol. Sci.* **2003**, *2* (5), 591−596.
(46) Ito, S.; Murakami, T. N.; Comte, P.; Liska, P.; Grätzel, C.; Nazeeruddin, M. K.; Grätzel, M. *Thin Solid Films* **2008**, *516* (14), 4613−4619.
(47) Wang, L. Z.; Sakai, N.; Ebina, Y.; Takada, K.; Sasaki, T. *Chem. Mater.* **2005**, *17* (6), 1352−1357.
(48) Wang, L. Z.; Omomo, Y.; Sakai, N.; Fukuda, K.; Nakai, I.; Ebina, Y.; Takada, K.; Watanabe, M.; Sasaki, T. *Chem. Mater.* **2003**, *15* (15), 2873−2878.
(49) Grätzel, M. *J. Photochem. Photobiol., A* **2004**, *164* (1−3), 3−14.
(50) Harms, H. A.; Tetreault, N.; Gusak, V.; Kasemo, B.; Gratzel, M. *Phys. Chem. Chem. Phys.* **2012**, *14* (25), 9037−9040.
(51) Zhang, H.; Han, Y.; Liu, X.; Liu, P.; Yu, H.; Zhang, S.; Yao, X.; Zhao, H. *Chem. Commun.* **2010**, *46* (44), 8395−8397.
(52) Yella, A.; Lee, H.-W.; Tsao, H. N.; Yi, C.; Chandiran, A. K.; Nazeeruddin, M. K.; Diau, E. W.-G.; Yeh, C.-Y.; Zakeeruddin, S. M.; Grätzel, M. *Science* **2011**, *334* (6056), 629−634.
(53) Choy, J.-H.; Lee, H.-C.; Jung, H.; Hwang, S.-J. *J. Mater. Chem.* **2001**, *11* (9), 2232−2234.
(54) Gunjakar, J. L.; Kim, I. Y.; Lee, J. M.; Lee, N.-S.; Hwang, S.-J. *Energy Environ. Sci.* **2013**, *6* (3), 1008−1017.
(55) Tan, B.; Wu, Y. Y. *J. Phys. Chem. B* **2006**, *110* (32), 15932−15938.
(56) Zhang, Q. F.; Dandeneau, C. S.; Zhou, X. Y.; Cao, G. Z. *Adv. Mater.* **2009**, *21* (41), 4087−4108.
(57) Pang, S.; Xie, T. F.; Zhang, Y.; Wei, X.; Yang, M.; Wang, D. J.; Du, Z. L. *J. Phys. Chem. C* **2007**, *111* (49), 18417−18422.
(58) Du, A. J.; Ng, Y. H.; Bell, N. J.; Zhu, Z. H.; Amal, R.; Smith, S. C. *J. Phys. Chem. Lett.* **2011**, *2* (8), 894−899.
(59) Ito, S.; Liska, P.; Comte, P.; Charvet, R.; Pechy, P.; Bach, U.; Schmidt-Mende, L.; Zakeeruddin, S. M.; Kay, A.; Nazeeruddin, M. K.; Gratzel, M. *Chem. Commun.* **2005**, *34*, 4351−4353.
(60) Huang, S. Y.; Schlichthorl, G.; Nozik, A. J.; Gratzel, M.; Frank, A. J. *J. Phys. Chem. B* **1997**, *101* (14), 2576−2582.
(61) Gregg, B. A.; Pichot, F.; Ferrere, S.; Fields, C. L. *J. Phys. Chem. B* **2001**, *105* (7), 1422−1429.

(62) Zaban, A.; Greenshtein, M.; Bisquert, J. *ChemPhysChem* **2003**, *4* (8), 859−864.
(63) Kuang, D.; Uchida, S.; Humphry-Baker, R.; Zakeeruddin, S. M.; Grätzel, M. *Angew. Chem., Int. Ed.* **2008**, *47* (10), 1923−1927.
(64) Liao, J.-Y.; Lin, H.-P.; Chen, H.-Y.; Kuang, D.-B.; Su, C.-Y. *J. Mater. Chem.* **2012**, *22* (4), 1627−1633.